Chemical Physics Letters 591 (2014) 78–81

Contents lists available at ScienceDirect

Chemical Physics Letters

journal homepage: www.elsevier.com/locate/cplett

Synthesis of graphene from dry ice in flames and its application in supercapacitors

Juan Zhang [a,b], Tian Tian [a], Youhu Chen [a], Yufang Niu [a], Jie Tang [c], Lu-Chang Qin [a,d,*]

[a] Division of Functional Materials and Nano-Devices, Ningbo Institute of Materials Technology and Engineering, Chinese Academy of Sciences, Ningbo 315201, China
[b] School of Materials Science and Chemical Engineering, Ningbo University, Ningbo 315201, China
[c] National Institute for Materials Science, Tsukuba 305-0043, Japan
[d] Department of Physics and Astronomy, University of North Carolina at Chapel Hill, Chapel Hill, NC 27599-3255, USA

ARTICLE INFO

Article history:
Received 10 October 2013
In final form 8 November 2013
Available online 15 November 2013

ABSTRACT

We have synthesized graphene by reducing carbon dioxide in magnesium and calcium metal flames. The as-prepared graphene has been used as conductive additive to improve the electrical conduction of activated carbon-based supercapacitor electrodes. The graphene/activated carbon composite electrode showed an outstanding specific capacitance of 220 and 180 F g^{-1} at a current density of 0.1 A g^{-1} in 6 M KOH electrolyte when using graphene obtained in magnesium and calcium flames, respectively.

1. Introduction

Supercapacitors based on the electrochemical double-layer capacitance are intermediate systems between electrochemical batteries and dielectric capacitors that utilize the double-layer formed at electrode/electrolyte interface to store and release energy [1,2]. Supercapacitors have been well recognized as important energy storage devices because of their pulse power supply, simple operation, long cycle life (>100,000 cycles), and high dynamics of charge propagation [3,4]. With a high power capability and a relatively high energy density compared to conventional capacitors, supercapacitors have been widely employed in complementing or replacing batteries in many applications involving energy storage and management systems [1,4].

At present, considerable efforts have been dedicated to exploring the high-performance carbon nanomaterials as electrodes of supercapacitors, owing to their excellent properties including stable electrochemical behavior, good cycle performance, and low cost [1]. On the other hand, as a unique carbon nanomaterial, the two-dimensional (2D) graphene with one-atom thickness is becoming a promising electrode material for fabricating high-performance supercapacitors because of its excellent electrical conductivity (>5000 S m^{-1}), mechanical stability and flexibility, and exceptionally large specific surface area (2630 m^2 g^{-1}) and supercapacitors based on graphene and its composites have actually been developed recently [5–10].

Various experimental methods for scalable production of graphene have been developed in recent years. Of particular interest are methods including chemical reduction of exfoliated graphite oxide (graphene oxide), electrochemical exfoliation of graphite, chemical vapor deposition, and chemical reduction in metal flames [11–16].

In this Letter, we report the synthesis of graphene by reducing CO_2 in magnesium and calcium flames and the structural and electrochemical characterization of the thus obtained graphene for supercapacitor applications. The graphene structure and physical properties were characterized by transmission electron microscopy (TEM), scanning electron microscopy (SEM), X-ray diffraction (XRD), and Raman spectroscopy. Electrochemical characterization used cyclic voltammetry (CV), electrochemical impedance spectroscopy (EIS), and galvanostatic charge–discharge (GC) to study and evaluate the electrochemical performance of the as-prepared graphene as conductive additive in assembled carbon supercapacitors.

2. Experimental

2.1. Preparation of carbon materials

Preparation of graphene was carried out using active metals (Mg and Ca) and CO_2 as carbon precursor. By burning Mg and Ca metals in a CO_2 atmosphere, graphene was produced in the following reactions that took place during the process.

$$2Mg(s) + CO_2(g) = 2MgO(s) + C(s) \quad (1)$$

$$2Mg(s) + O_2(g) = 2MgO(s) \quad (2)$$

* Corresponding author at: Department of Physics and Astronomy, University of North Carolina at Chapel Hill, Chapel Hill, NC 27599-3255, USA. Fax: +1 919 962 0480.
E-mail address: lcqin@email.unc.edu (L.-C. Qin).

0009-2614/$ - see front matter © 2013 Elsevier B.V. All rights reserved.
http://dx.doi.org/10.1016/j.cplett.2013.11.014

and

$$2Ca(s) + CO_2(g) = 2CaO(s) + C(s) \quad (3)$$

$$2Ca(s) + O_2(g) = 2CaO(s) \quad (4)$$

After the explosive reactions, we collected the black graphene powders and transferred them to a beaker filled with 10% HCl to remove the metallic oxide and unreacted metal. The mixture was then vacuum filtered using polypropylene membrane with pore size of 0.45 μm and washed with deionized water. The processed graphene material was finally obtained after the resultant residues were dried in vacuum overnight at room temperature.

2.2. Structural characterization

Scanning electron microscopy (SEM, Hitachi S4800) and transmission electron microscopy (TEM, Tecnai F20) were used to examine the morphology of all samples. X-ray diffraction (XRD) was carried out using a D8 Advance (Bruker) diffractometer with Cu K_α radiation (λ = 0.15418 nm) to evaluate the crystallization of graphene. Raman spectroscopy (Thermo Scientific DXR) measurement using 532 nm laser was also performed to characterize the disorder and defects in graphene.

2.3. Construction of supercapacitors and electrochemical characterization

We used a two-electrode configuration to evaluate the electrochemical performance of the active electrode material in the constructed supercapacitors. The supercapacitor cells were assembled according to the reported method [3,17]. The electrode material consists of activated carbon matrix material, conductive additive, and polytetrafluoroethylene (PTFE) binder. The carbon paste was painted on current collectors. To construct a symmetric supercapacitor, two identical electrodes were separated by a glass fiber film and sandwiched in a stainless steel cell (CR2016).Electrochemical performance of the supercapacitor was examined by cyclic voltammetry (CV), electrochemical impedance spectroscopy (EIS), and galvanostatic charge–discharge (GC) using a Zahner-zennium electrochemical workstation. The applied potential range for CV measurement was –1 to 0 V with scan rates varying from 10 to 200 mV s^{-1}. EIS measurement was carried out at an open circuit voltage with a sinusoidal signal of 5 mV over the frequency range of 100 mHz–100 kHz. GC measurement at different constant current densities varying from 0.1 to 2.0 A g^{-1} was performed at charging voltage of 1 V.

3. Results and discussion

3.1. Structural characterization

The obtained graphene material was fully analyzed by transmission electron microscopy (TEM) and scanning electron microscopy (SEM). Figure 1a shows a low magnification TEM image of the as-prepared graphene sample, in which the morphology of the graphene sheets is seen as superimposed squares and their sizes are typically between 50 and 200 nm. The TEM image of graphene sheets shown in Figure 1b reveals a typical sheet-like structure with fewer than five monolayers of graphene. Larger stacks of few-layer graphene sheets are shown in Figure 1c, where the graphene sheets are scrolled and entangled. The selected-area electron diffraction (SAED) pattern of graphene sheets is given as the inset in Figure 1c, where the (100) and (200) Bragg reflections from graphene are clearly shown while the (002) reflection is weak and diffused, attributing to the poor order in stacking and the few-layered structure. Figure 1d shows the TEM image of MgO crystals after the reactions completed. The MgO crystals exhibit cubic morphology with edge length of about 50 nm. As observed in Figure 1a, the similar morphology of the graphene sheets indicates that the graphene was grown on the template MgO crystals [12,18]. From the SEM images of the as-prepared graphene shown in Figure 1e and f, the cubic morphology of graphene was also revealed with length of 50–200 nm in agreement with the TEM observations. Therefore, the MgO crystals served as templates for deposition of carbon and formation of graphene during the reactions.

Figure 2 shows the X-ray diffraction pattern of the graphene material prepared by using Mg as the reductant and CO_2 as the oxidant. A relatively weak and broad graphitic (002) reflection at 2θ = 26.4°, corresponding to an inter-layer spacing of about 0.34 nm, is observed along with two additional peaks attributed largely to the {200} and {220} reflections of MgO appeared at 43.2° and 62.6°, respectively. It should also be noted that the (100) reflection due to graphene coincides with the {200} reflection of MgO. The presence of the graphitic (002) peak in the XRD pattern indicates that multilayer graphene must have also been produced in the process.

Raman spectroscopy is a powerful technique for characterizing graphene material, because it can reveal fine structural and

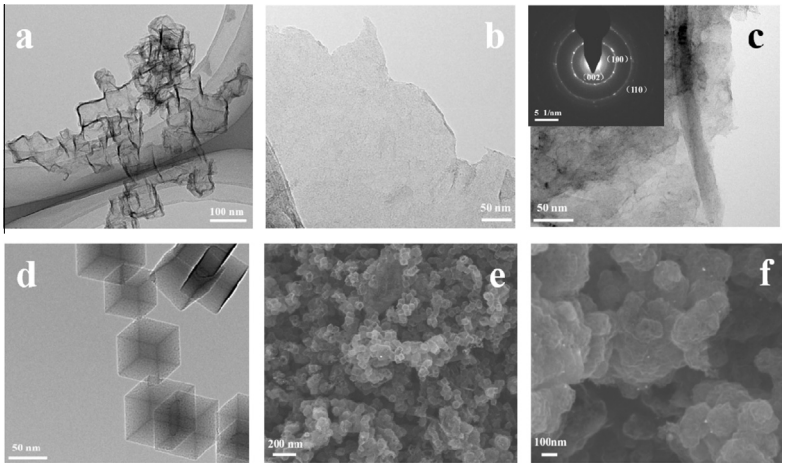

Figure 1. (a–c) TEM images of graphene prepared from chemical reactions in flames using magnesium metal and carbon dioxide as precursor. The inset in (c) is the SAED pattern, confirming the crystalline nature of the as-prepared graphene material; (d) TEM image of cubic MgO crystals; (e–f) SEM images of as-prepared graphene material.

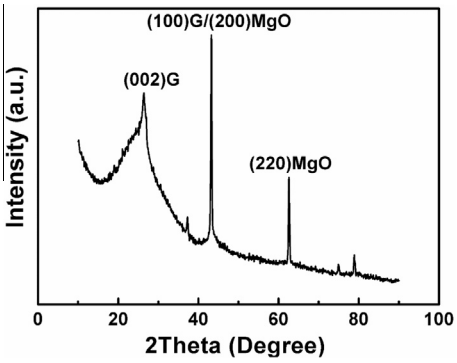

Figure 2. X-ray diffraction pattern of graphene using Mg as chemical reactant. The broadened (002) reflection is due to graphene and the sharp (200) and (220) reflections are due to MgO crystals.

electronic information including disorder and defect structures in graphene [19,20]. We acquired Raman spectra using 532 nm radiation. In the Raman spectrum there are three main characteristic peaks, the D band arising from an in-plane breathing vibration mode, and the G band resulting from the doubly degenerate in-plane vibration mode, resulting in two peaks at about ~1580 and ~1350 cm^{-1}, respectively [19,20]. The other most prominent peak is the 2D band at ~2700 cm^{-1}, which has been used to distinguish monolayer, bilayer, and few-layer graphene on the basis of the position and shape of the 2D band [20].

Figure 3 shows the Raman spectrum of the graphene material prepared from the chemical reactions using magnesium metal and carbon dioxide as precursor. The G band is broadened and shifted upward to around 1582 cm^{-1}, while the intensity of the D band at 1339 cm^{-1} showed a higher intensity. Though the observed Raman shift of the D band varies with the laser wavelength, the appearance of the D band is related to the structural disorder at defect sites [21]. The area ratio of the D band to G band is correlated with the disordered structure and the ratio will increase with increasing disorder [22]. As shown in Figure 3, the Raman spectrum has a much stronger D band with the D to G area ratio of 1.71, attributing to a high concentration of defects and disorders at the edges. It should be noted that much lower concentrations of defects were observed in graphene samples produced by reducing CO_2 in Ca flames or electrochemical exfoliation [14] in which the relative peak heights of the D and G bands are reversed. The peak position of the 2D band of the graphene material shown in Figure 3 (2670 cm^{-1}) was slightly downshifted compared to those of the reported value for graphene (2700 cm^{-1}) and graphite

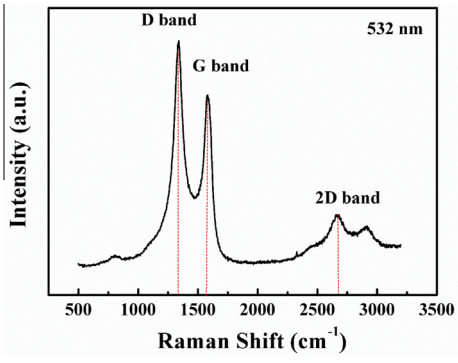

Figure 3. Raman spectra at 532 nm of as-prepared carbon material showing a D band at 1339 cm^{-1}, a G band at 1582 cm^{-1}, and a 2D band at 2670 cm^{-1}.

(2687 cm^{-1}). As already reported in the literature, the monolayer graphene sheets will give rise to a single and sharp 2D peak located below 2700 cm^{-1}, while the bilayer graphene sheets have a broader 2D peak at 2700 cm^{-1} and graphene sheets with more than five layers have a broad 2D peak with the positions significantly shifted to above 2700 cm^{-1} [19,20]. Therefore, the Raman spectrum given in Figure 3 indicates that the graphene obtained in our experiment has typically fewer than five graphene layers.

3.2. Electrochemical characterization

The as-prepared graphene has been used as conductive additive in activated carbon electrodes and the supercapacitor performance was evaluated by cyclic voltammetry (CV), electrochemical impedance spectroscopy (EIS), and galvanostatic charge–discharge (GC). Figure 4a is the CV curves of the supercapacitor based on activated carbon (AC) electrodes incorporating with the as-prepared graphene produced in Mg flames (G(Mg)/AC, red) and Ca flames (G(Ca)/AC, black), respectively, in 6 M KOH aqueous electrolyte at the scan rate of 50 mV^{-1}. The characteristic rectangular shape of the CV loop indicates excellent charge propagation at the electrode–electrolyte interface according to the energy storage mechanism of electric double-layer capacitors (EDLC) [23,24]. Furthermore, the faradic pseudo-capacitance caused by functional groups on the electrode surface can be neglected because there were no apparent peaks due to faradaic oxidation–reduction current between −1 and 0 V [24]. Figure 4b shows the typical charge and discharge curves for G(Mg)/AC (red) and G(Ca)/AC (black), respectively, in 6 M KOH aqueous electrolyte at the current density of 0.1 A g^{-1}. The linear profile of galvanostatic charge–discharge curves and their symmetric triangular shape indicate nearly ideal capacitive characteristics.

The specific capacitance of supercapacitor electrode is calculated from the galvanostatic discharge curve using the following equation [17]

$$C_{2E}^{spec} = \frac{4I_{cons}}{MdV/dt}, \quad (5)$$

where C_{2E}^{spec} is the specific capacitance of the electrode, I_{cons} is the constant current, dV/dt is the slope of discharge curve obtained through linear fitting, and M is the total weight of two symmetrical electrodes. At the constant current density of 0.1 A g^{-1}, the specific capacitance of G(Mg)/AC and G(Ca)AC was 220 and 185 F g^{-1}, respectively. When the constant current density was increased to 2.0 A g^{-1}, the specific capacitance was 186 and 147 F g^{-1} for G(Mg)/AC and G(Ca)/AC, respectively. The apparent difference in specific capacitance of G(Mg)/AC and G(Ca)/AC is attributed to their structural differences. G(Ca)/AC is structurally closer to graphite - it contains more graphene layers and fewer defects. The rate performance of the supercapacitor electrode was also evaluated by galvanostatic charge–discharge under increased current density and the result is shown in Figure 4c. As shown in Figure 4c, the G(Mg)/AC composite electrode preserved 85% of its specific capacitance when the charging current increased from 0.1 to 2.0 A g^{-1}, which is slightly higher than that of the G(Ca)/AC composite electrode. The fact that the specific capacitance will decrease with increasing current density is attributed to higher internal resistance and slower electrolyte diffusion in the electrode [25]. This is also confirmed by the Nyquist plots obtained from the EIS data given in Figure 4d. At low frequency, the straight line is nearly perpendicular to the real axis Z', indicating a pure capacitive behavior and that the electrolyte ions had completely diffused into the interior of the electrode material [3]. As the frequency increased, the influence of the electrode porosity was observed. When the frequency decreases, starting from very high frequency, the signal penetrates

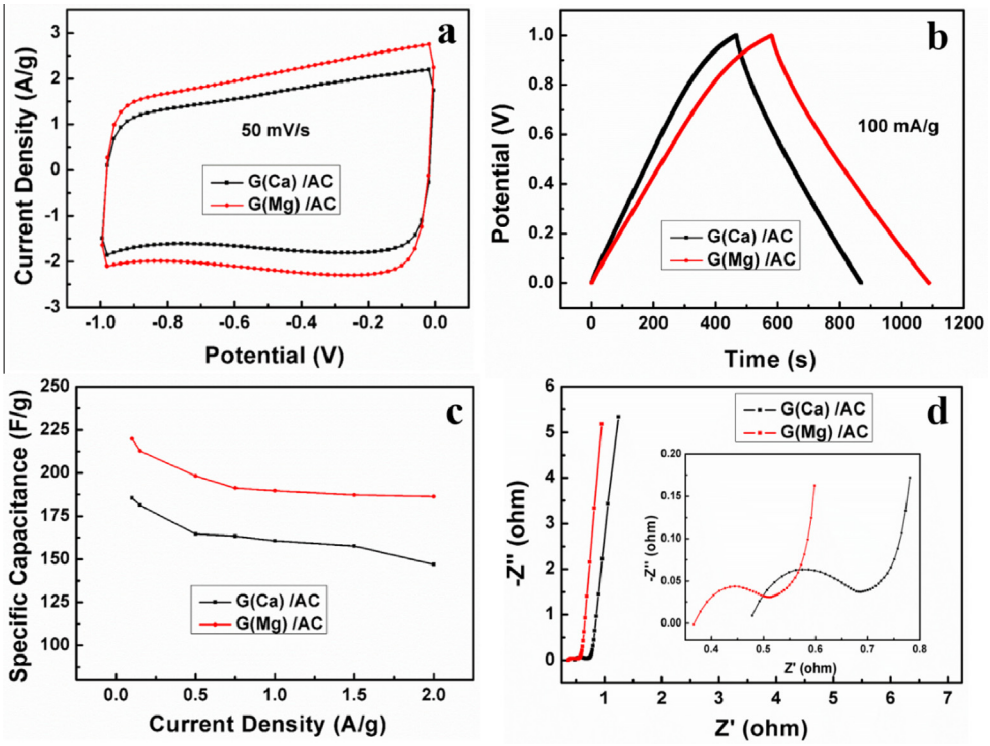

Figure 4. Electrochemical characterization of G(Mg)/AC and G(Ca)/AC supercapacitor electrodes. (a) CV curves at scan rate of 50 mV s^{-1}; (b) GC curves at constant current density of 100 mA g^{-1}; (c) Specific capacitance obtained from GC curves at different current densities varying from 0.1 to 2.0 A g^{-1}; (d) Nyquist plots of EIS data.

deeper and deeper into the porous structure of electrode, and then more and more electrode surface becomes approachable for ion adsorption [17]. There is also a domain in a small frequency range, where a straight line with a 45° angle is observed, resulting from the diffusion of electrolyte ions (Warburg impedance) [3,17,25]. It is well known that the higher frequency the Warburg curve starts, the more easily the electrolyte penetrates into the porous structure of the electrode. From the inset given in Figure 4d, it can be seen that the starting frequency of the Warburg curve for G(Mg)/AC electrode is 1332 Hz, which is higher than that for G(Ca)/AC (674 Hz). This result also confirms that the G(Mg)/AC electrode has better rate capability. Moreover, the charge transfer resistance R_t of G(Mg)/AC electrode, which reflected the inter-granular contact resistance between AC particles and graphene sheets, is smaller, also implying easier diffusion of the electrolyte ions [17]. The semi-circle observed in the high frequency range where the equivalent series resistance (ESR) is obtained by extrapolating the straight line to intercept the real axis Z' [25]. The ESR of G(Mg)/AC and G(Ca)/AC are 0.366 and 0.478 Ω, respectively, indicating a smaller intrinsic resistance of G(Mg)/AC and also a lower contact resistance at the interface between the active material and current collector [3].

4. Conclusions

We have synthesized graphene by the chemical reactions between Mg/Ca metal and dry ice (CO_2) and have characterized and improved the electrochemical performance of carbon supercapacitors when the graphene was used as conductive additive. High specific capacitance of 220 F g^{-1} in activated carbon electrode incorporating with the as-prepared graphene has been obtained at the constant current density of 0.1 A g^{-1}, which is much higher than that of electrodes made of activated carbon incorporated with carbon blacks or graphite powders.

Acknowledgement

J.T. wishes to thank the JST ALCA Program (Japan) for financial support.

References

[1] A.G. Pandolfo, A.F. Hollenkamp, J. Power Sources 157 (2006) 11.
[2] L.L. Zhang, X. Zhao, Chem. Soc. Rev. 38 (2009) 2520.
[3] J. Gamby, P. Taberna, P. Simon, J. Fauvarque, M. Chesneau, J. Power Sources 101 (2001) 109.
[4] S. Bose, T. Kuila, A.K. Mishra, R. Rajasekar, N.H. Kim, J.H. Lee, J. Mater. Chem. 22 (2012) 767.
[5] M.D. Stoller, S. Park, Y. Zhu, J. An, R.S. Ruoff, Nano. Lett. 8 (2008) 3498.
[6] S. Vivekchand, C.S. Rout, K. Subrahmanyam, A. Govindaraj, C. Rao, J. Chem. Sci. 120 (2008) 9.
[7] Q. Cheng, J. Tang, N. Shinya, L.-C. Qin, J. Power Sources 241 (2013) 423.
[8] Q. Cheng, J. Tang, J. Ma, H. Zhang, N. Shinya, L.-C. Qin, Phys. Chem. Chem. Phys. 13 (2011) 17615.
[9] Q. Cheng, J. Tang, J. Ma, H. Zhang, N. Shinya, L.-C. Qin, Carbon 49 (2011) 2917.
[10] K. Novoselov et al., Science 306 (2004) 666.
[11] Y. Hernandez et al., Nat. Nanotechnol. 3 (2008) 563.
[12] G. Ning, Z. Fan, G. Wang, J. Gao, W. Qian, F. Wei, Chem. Commun. 47 (2011) 5976.
[13] Y. Huang, J. Liang, Y. Chen, Small 8 (2012) 1805.
[14] M. Zhou, J. Tang, Q. Cheng, G. Xu, P. Cui, L.-C. Qin, Chem. Phys. Lett. 572 (2013) 61.
[15] M. Zhou et al., Chem. Phys. Lett. 581 (2013) 64.
[16] A. Chakrabarti, J. Lu, J.C. Skrabutenas, T. Xu, Z. Xiao, J.A. Maguire, N.S. Hosmane, J. Mater. Chem. 21 (2011) 9491.
[17] C. Portet, P. Taberna, P. Simon, C. Laberty-Robert, Electrochim. Acta 49 (2004) 905.
[18] M.H. Rummeli et al., ACS Nano 4 (2010) 4206.
[19] A.C. Ferrari, Solid State Commun. 143 (2007) 47.
[20] A. Ferrari et al., Phys. Rev. Lett. 97 (2006) 187401.
[21] Y. Wang, D.C. Alsmeyer, R.L. McCreery, Chem. Mater. 2 (1990) 557.
[22] A. Ferrari, J. Robertson, Phys. Rev. B 61 (2000) 14095.
[23] B. Conway, Electrochemical Supercapacitors: Scientific Fundamentals and Technological Applications, Kluwer Academic/Plenum, New York, 1999.
[24] J. Chen, W. Li, D. Wang, S. Yang, J. Wen, Z. Ren, Carbon 40 (2002) 1193.
[25] P. Taberna, P. Simon, J.-F. Fauvarque, J. Electrochem. Soc. 150 (2003) A292.